Journal of Materials Chemistry C

PAPER

View Article Online
View Journal | View Issue

Cite this: J. Mater. Chem. C, 2015, 3, 10422

$MoSi_2$-type narrow band gap intermetallic compound $Al_6Re_5Si_4$ as a thermoelectric material

Y. Takagiwa,*[ab] S. Utada,[c] I. Kanazawa[c] and K. Kimura[a]

Received 3rd June 2015,
Accepted 23rd June 2015

DOI: 10.1039/c5tc01608h

www.rsc.org/MaterialsC

The thermoelectric properties of $MoSi_2$-type intermetallic compound $Al_6Re_5Si_4$ (investigated compositions: $Al_{6-x}Re_{4.7}Si_{4+x}$ (x = 0–0.9)) related to $TiSi_2$-type narrow band gap intermetallic compounds were systematically investigated. A first-principles band structure calculation implies that this compound forms a narrow band gap in the electronic density of states that will be suitable for obtaining a large power factor. Indeed, the maximum power factor is 1.65 mW m^{-1} K^{-2} for the sample with x = 0.8. The $Al_{6-x}Re_{4.7}Si_{4+x}$ (x = 0–0.8) samples show degenerate semiconductor behavior as p-type materials; the temperature coefficient of the electrical conductivity is negative and the positive Seebeck coefficient increases with increasing temperature. A negative Seebeck coefficient is observed in the Si-rich sample with x = 0.9, which is understood by shifting the Fermi level to the conduction band. The estimated band gap is 0.53 eV from the Arrhenius plot. Because of a simple crystal structure, a relatively high thermal conductivity ranging from 7.6 to 13.5 W m^{-1} K^{-1} is observed at 300 K. The maximum dimensionless figure-of-merit of 0.19 at 973 K is close to the optimal value predicted by a single parabolic band model.

1. Introduction

To date, building a sustainable energy society using natural and renewable energy sources instead of non-renewable fossil fuels remains an unsolved issue. One of the promising contributions is thermoelectric power generation through the direct conversion of waste heat into electrical energy.[1] Its efficiency is closely related to the dimensionless figure-of-merit, zT, defined as $zT = S^2\sigma T/\kappa_{total}$, where S, σ, κ_{total}, and T are the Seebeck coefficient, the electrical conductivity, the total thermal conductivity, and the temperature, respectively. The κ_{total} consists of two contributions; the phonon part, κ_{phonon}, and the electron part, $\kappa_{electron}$. Much effort for improving efficiency and finding new materials has been performed, based on novel concepts for zT enhancement such as resonance states at the band edge,[2] band structure engineering,[3] and introduction of nanostructures.[4]

One of the criteria for a new material is a narrow band gap compound possessing a large power factor, $S^2\sigma$, and/or a low thermal conductivity. In general, $S^2\sigma$ depends on the local electronic structure near the Fermi level, E_F. Most promising thermoelectric materials, such as lead chalcogenides,[5] clathrates,[6] and skutterudites,[7] form narrow band gaps near the E_F. On the other hand, a glass-like low κ_{phonon} will be obtained in solids with complex crystal structures.[8,9]

Recently, narrow band gap binary intermetallic compounds composed of group-13 and transition metal elements have been extensively investigated as a new class of thermoelectric materials: $TiSi_2$-type $RuAl_2$,[10–12] $RuGa_2$,[12–19] $FeGa_3$-type $RuGa_3$,[20,21] $RuIn_3$,[21–25] and $FeGa_3$.[20,26–29] In particular, $RuAl_2$ and $RuGa_2$ have been shown to have one of the Nowotny chimney-ladder phases with a valence electron concentration of approximately 14.[30] zT enhancement is achieved through carrier doping by suitable elemental substitutions. The highest zT values for p- and n-type in these compounds are 0.80 and 0.31 for Sn-doped $RuIn_3$[23] and Ir-doped $RuGa_2$,[17] respectively. Recently, Takeuchi *et al.* reported the thermoelectric properties of related ternary low-cost $TiSi_2$-type Al–Mn–Si compounds (zT_{300K} = 0.05)[31] and demonstrated a zT enhancement up to 0.38 with n-type Ru and Re co-substitutions with the composition of $Al_{37.0}(Mn_{26.0}Ru_{3.0}Re_{3.0}Fe_{1.0})Si_{30.0}$.[32] Very recently, the thermoelectric properties of $CrSi_2$-type W or Ta containing Al–Mn–Si have been reported.[33]

In this study, we focus on a related $MoSi_2$-type compound, $Al_6Re_5Si_4$, possessing a tetragonal crystal structure (the space group: $I4/mmm$ with lattice parameters of $a(b)$ = 3.180 Å and c = 8.020 Å).[34] It contains mixing sites of Al/Si, as shown in Fig. 1. To date, there have been few reports on $Al_6Re_5Si_4$ that include phase stability, electronic structure, and physical properties. The purpose of this work is characterizing the band structure and the thermoelectric properties of $MoSi_2$-type $Al_6Re_5Si_4$ and discussing the properties in terms of a single parabolic band

[a] Department of Advanced Materials Science, The University of Tokyo, 5-1-5 Kashiwanoha, Kashiwa, Chiba 277-8561, Japan
[b] National Institute for Materials Science, 1-2-1 Sengen, Tsukuba, Ibaraki 305-0047, Japan. E-mail: TAKAGIWA.Yoshiki@nims.go.jp; Tel: +81-29-859-2811
[c] Department of Physics, Tokyo Gakugei University, 4-1-1 Nukuikitamachi, Koganei, Tokyo 184-8501, Japan

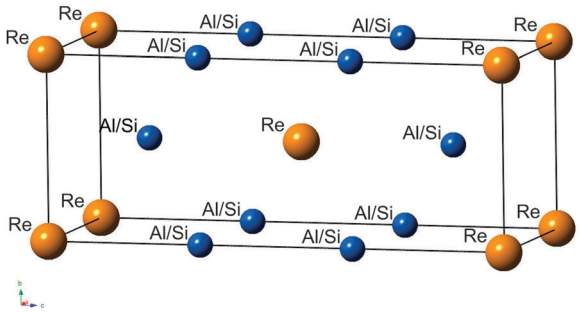

Fig. 1 Crystal structure of $MoSi_2$-type $Al_6Re_5Si_4$. The blue and orange spheres are Al(0.6)/Si(0.4) and Re, respectively.

model, which contribute to enhance our insight upon further zT improvement for ternary Al–(Mn,Re)–Si systems.

2. Experimental procedure and phase characterization

First, we determined the single-phase composition range of $Al_6Re_5Si_4$. Nominal compositions of $Al_6Re_{5-\delta}Si_4$ (δ = 0, 0.3, and 0.5) were selected. Cold-pressed pellet samples from a mixture of powder Al (4N purity; Kojundo Chemical Laboratory Co. Ltd, Tokyo, Japan), Re (4N purity; Rare Metallic Co. Ltd, Tokyo, Japan), and Si (4N purity; Kojundo Chemical Laboratory Co. Ltd, Tokyo, Japan) were arc-melted (NEV-ACD-05; Nissin Giken Co., Saitama, Japan) under an argon atmosphere, followed by spark plasma sintering (SPS) (SPS-515S; Fuji Electronic Industrial Co., Kanagawa, Japan). The obtained button shape samples were crushed into fine powder with particles sizes below 45 μm with an agate mortar for sintering. The powder samples were set in a 10 mm-diameter carbon die with carbon spacers. The temperature of the specimen was increased from room temperature to 1873–1973 K with uniaxial pressure of 115 MPa under an argon atmosphere, and the consolidating temperature was then held for 10 min. The characterization of the samples was performed by X-ray diffraction measurements using Cu Kα radiation (SmartLab; Rigaku Co., Tokyo, Japan).

Fig. 2 shows the X-ray diffraction patterns of $Al_6Re_{5-\delta}Si_4$ (δ = 0, 0.3, and 0.5) after arc melting. Because the stoichiometric composition of $Al_6Re_5Si_4$ (δ = 0) contains Re as a secondary phase, we obtained a single-phase sample in the slightly off-stoichiometric composition of $Al_6Re_{4.7}Si_4$ (δ = 0.3). Further decreasing the Re concentration leads to the secondary phase of α-Al–Re–Si.[35] Therefore, we selected the nominal composition of $Al_6Re_{4.7}Si_4$ as a starting point. Considering the crystal structure of $Al_6Re_5Si_4$ (see Fig. 1), introducing vacancies at Re sites would be unstable and lead to apparent Re reduction brought about by reducing Al and Si during the arc-melting process. Indeed, weight loss of about 2% was observed.

To tune the thermoelectric properties, we synthesized several $Al_{6-x}Re_{4.7}Si_{4+x}$ (x = −1.0 to 1.0) compounds with constant Re concentration. The sample preparation procedure is the same as that for $Al_6Re_{5-\delta}Si_4$. The obtained bulk samples are all highly dense, with relative densities of over 95%.

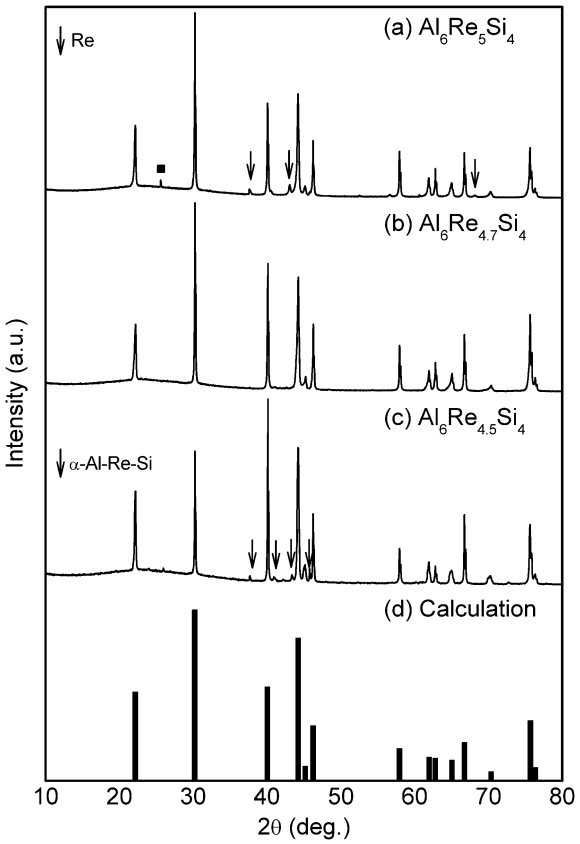

Fig. 2 (a–c) X-ray diffraction patterns for $Al_6Re_{5-\delta}Si_4$ (δ = 0, 0.3, and 0.5) after arc melting, together with calculated patterns (d). The arrows indicate (a) the secondary phases of Re and (c) the α-Al–Re–Si phase.[35] The square indicates an unidentified phase (a).

We found that samples with x = 0–0.8 are in the single phase, as shown in Fig. 3, together with calculated patterns. As for samples with $x > 0.8$ and $x < 0$ (not shown), extra peaks of secondary phases are observed, indicating that the solubility limit of Al/Si is limited within 5.5 at%, as presented in Fig. 4.

The electrical conductivity and the Seebeck coefficient were measured in a helium atmosphere between 373 K and 973 K using the four-probe method and the steady-state temperature gradient method, respectively (ZEM-1; Advance-Riko, Inc., Kanagawa, Japan). The thermal conductivity was obtained by measuring the geometric density, and specific heat and thermal diffusivity were obtained using the laser flash method (TC-7000; Advance-Riko, Inc.). Hall coefficient measurements were performed at room temperature (Resitest 8300, Toyo Co., Tokyo, Japan). The Debye temperatures were calculated from the transversal and longitudinal speed of sound measured using an ultrasonic pulse echo method (Echometer 1062; Nihon Matech Co., Tokyo, Japan).

3. Electronic density of states and band structure calculation

To clarify the electronic structure of $Al_6Re_5Si_4$, we performed a first-principles band structure calculation using the Advance/PHASE

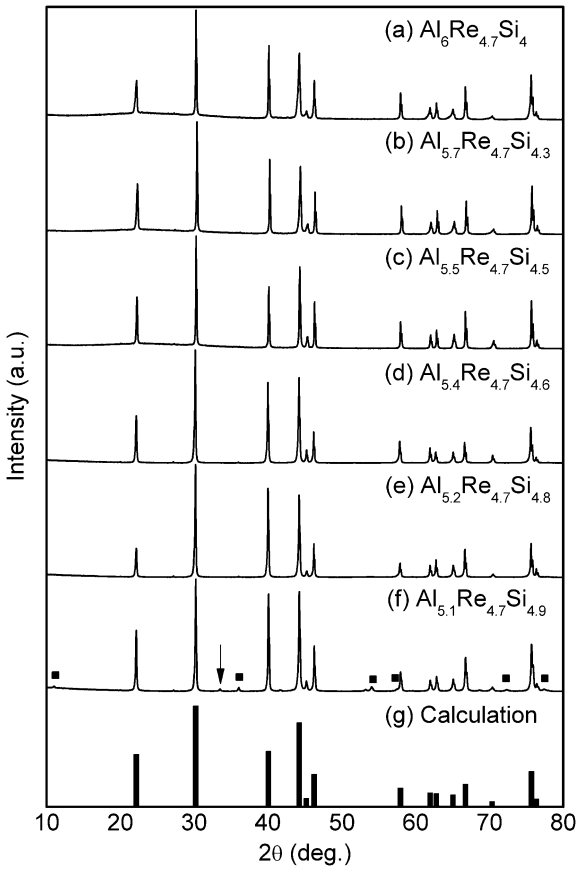

Fig. 3 (a–f) X-ray diffraction patterns for $Al_{6-x}Re_{4.7}Si_{4+x}$ (x = 0–0.9), together with calculated patterns (g). The arrow and squares indicate Si and an unidentified phase, respectively.

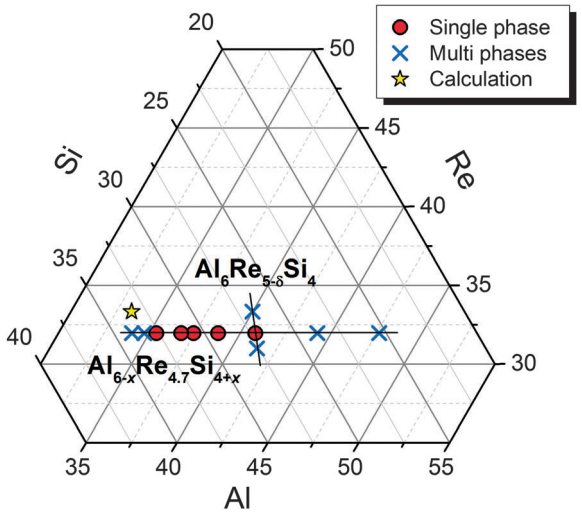

Fig. 4 Nominal composition diagram of synthesized $Al_6Re_{5-\delta}Si_4$ (δ = 0, 0.3, and 0.5) and $Al_{6-x}Re_{4.7}Si_{4+x}$ (x = −1.0 to 1.0). The circle, cross, and star symbols represent the compositions of single-phase, multiple-phases, and calculation (see Fig. 6(a)), respectively.

package program,[36] which employs projector augmented wave pseudopotentials within the generalized gradient approximation of density functional theory. It should be noted that $Al_6Re_5Si_4$ contains mixing sites of Al(0.6)/Si(0.4) (see Fig. 1),[34] which prevent the correct calculation of the electronic structure. Hence, we first adopted hypothetical ordered $ReAl_2$ and $ReSi_2$ with a tetragonal $MoSi_2$-type crystal structure for calculation. Because the crystal structure of $ReSi_2$ is recognized as an orthorhombic $MoPt_2$-type structure with lattice parameters of a = 3.128 Å, b = 3.144 Å, and c = 7.677 Å with the same atomic cordination,[37] we calculated the electronic density of states (DOS) using both $MoSi_2$- and $MoPt_2$-type crystal structures for $ReSi_2$. A dense mesh of 50 k-points in the whole Brillouin zone was used, and the cut-off energy of 340 eV was selected. After structural optimization with the constant lattice parameters, we obtained the DOS for both $ReAl_2$ and $ReSi_2$, as shown in Fig. 5. There is no significant difference in the DOS between $MoSi_2$- and $MoPt_2$-type $ReSi_2$.

The hypothetical $MoSi_2$-type $ReAl_2$ forms a band gap of 0.86 eV about 1 eV above E_F. In this case, $ReAl_2$ will have p-type metallic properties. In contrast, $ReSi_2$ has a wide pseudogap below E_F and shows n-type properties. These imply that the DOS and band gap are changing with Al/Si concentrations: non-rigid band like changes. Considering that $Al_6Re_5Si_4$ possesses an intermediate number of valence electrons between $ReAl_2$ and $ReSi_2$, E_F can be shifted to both valence and conduction bands by tuning the sample composition. Indeed, such

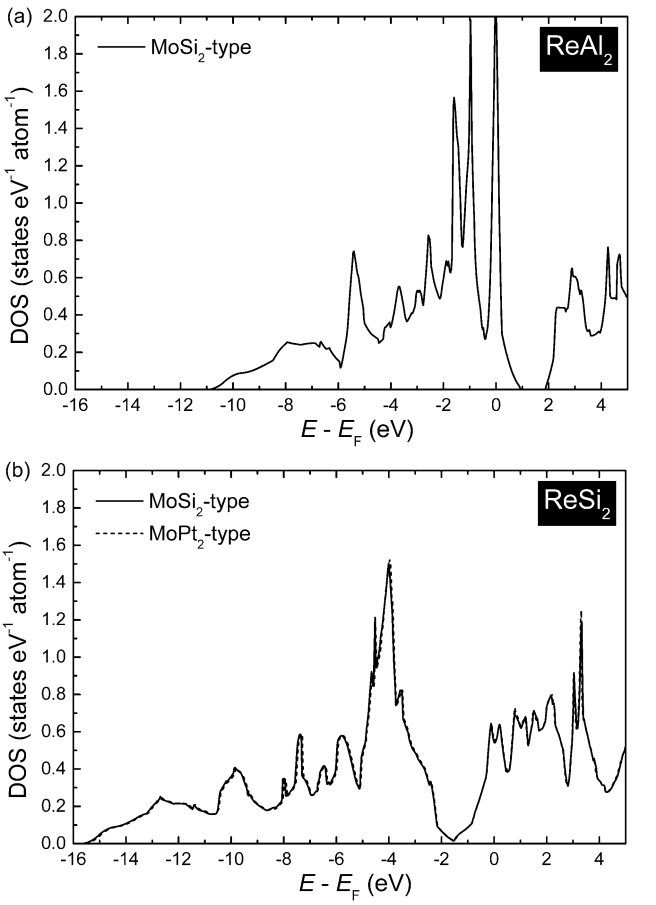

Fig. 5 Electronic density of states (DOS) for ordered (a) $MoSi_2$-type $ReAl_2$ and (b) $MoSi_2$- and $MoPt_2$-type $ReSi_2$.

optimization can be achieved by changing Al/Si concentrations, as described in the next section.

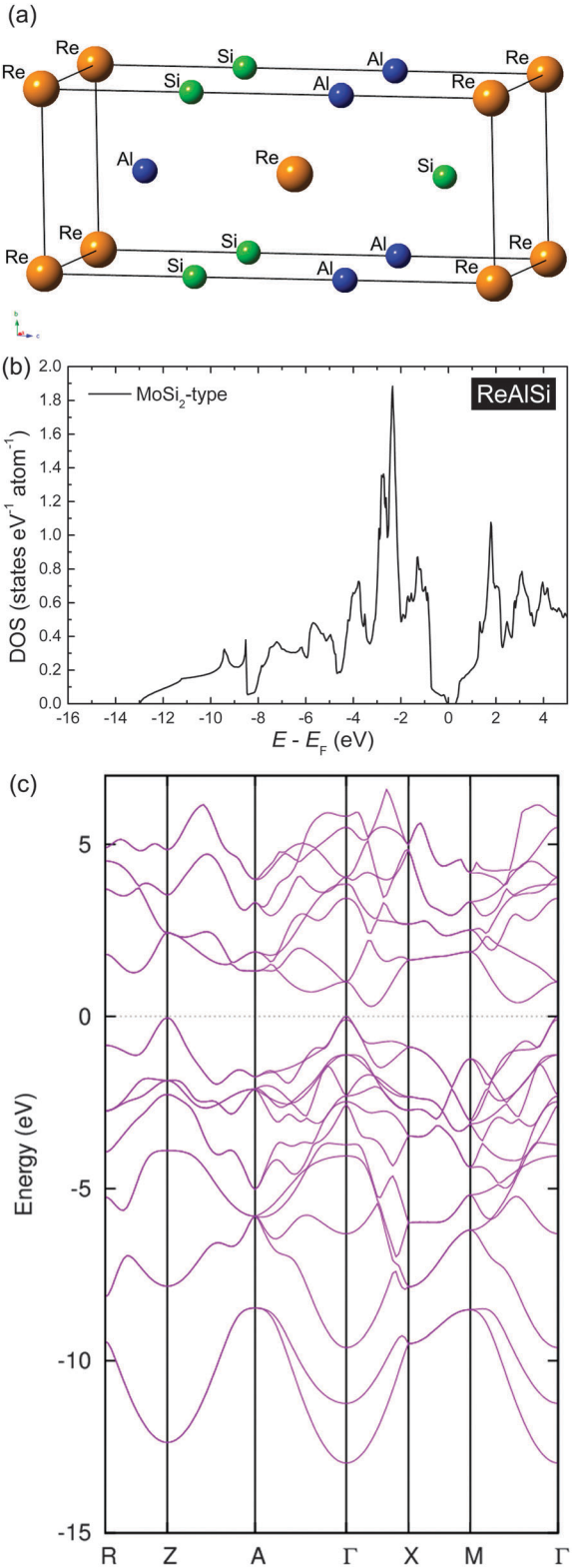

Fig. 6 (a) Crystal structure model, (b) electronic density of states (DOS), and (c) band structure for $MoSi_2$-type ReAlSi.

In addition to the above structural models, we constructed another hypothetical model of $MoSi_2$-type $Al_6Re_5Si_4$, *i.e.*, ReAlSi (Fig. 6a), which is similar to the experimental composition of the sample with $x = 1.0$, as displayed in Fig. 4. In this model, a dense mesh of 8000 k-points in the whole Brillouin zone was used. The DOS using this model is displayed in Fig. 6b, and a narrow band gap of 0.28 eV is observed. This value seems to be underestimated, compared with the experimentally obtained value of 0.53 eV, as described in the next section. From the electronic band structure (Fig. 6c), the obtained band gap is indirect and an effective band degeneracy of $N_v = 4$ is recognized. The parabolic shape of lighter valence bands and heavier conduction bands is realized. A parabolic fit to the top of the valence band at the gamma point yields the effective mass of $\sim 0.3m_e$.

4. Thermoelectric properties of $Al_{6-x}Re_{4.7}Si_{4+x}$ (x = 0–0.9)

Fig. 7a and b show the electrical conductivity, σ, and the Seebeck coefficient, S, as a function of temperature for $Al_{6-x}Re_{4.7}Si_{4+x}$ (x = 0–0.9). The thermoelectric properties are quite sensitive to the sample composition, which is generally observed in narrow band gap compounds. Indeed, the σ at 400 K ranges widely from 25 to 7300 Ω^{-1} cm^{-1}. The samples with x = 0–0.8 show degenerate semiconductor behavior, while the sample with x = 0.9 shows non-degenerate behavior. The σ decreases and the S increases with increasing x up to x = 0.8, indicating that the carrier concentration decreases monotonically by shifting E_F to the valence band edge. A further increase in x brings n-type transport properties with intrinsic semiconductor behavior. Using the data for x = 0.9, the estimated band gap is 0.53 eV from the Arrhenius plot above 800 K. This value is larger than that of the hypothetical model ReAlSi, as already mentioned in Section 2.

Fig. 7c plots the Hall carrier concentration, n_H, *versus* S for selected $Al_{6-x}Re_{4.7}Si_{4+x}$ (x = 0.6 and 0.8), using a single parabolic band (SPB) model[38] for the valence bands. This assumption would be reasonable, considering the band dispersion at the valence band maximum (VBM). Using the SPB model only for doping levels and temperatures where minority carrier effects are not observed in the transport data is necessary. In this sense, the samples with x = 0.9 should be excluded for analysis. The σ and S at 400 K are almost identical between the samples with x = 0.5 and 0.6. On the other hand, the S of the samples with x = 0 and 0.3 are of almost zero value. Thus, we selected the samples with x = 0.6 and 0.8 for analysis using the SPB model. This model assumes that acoustic phonons are the dominant scattering events ($\lambda = 0$). Using the following equations, we employed the SPB model at 373 K.

$$S = \frac{k_B}{e}\left\{\frac{(2+\lambda)F_{1+\lambda}(\eta)}{(1+\lambda)F_\lambda(\eta)} - \eta\right\}, \quad (1)$$

$$n = 4\pi\left(\frac{2m^* k_B T}{h^2}\right)^{3/2} F_{1/2}(\eta), \quad n_H = n/r_H, \quad (2)$$

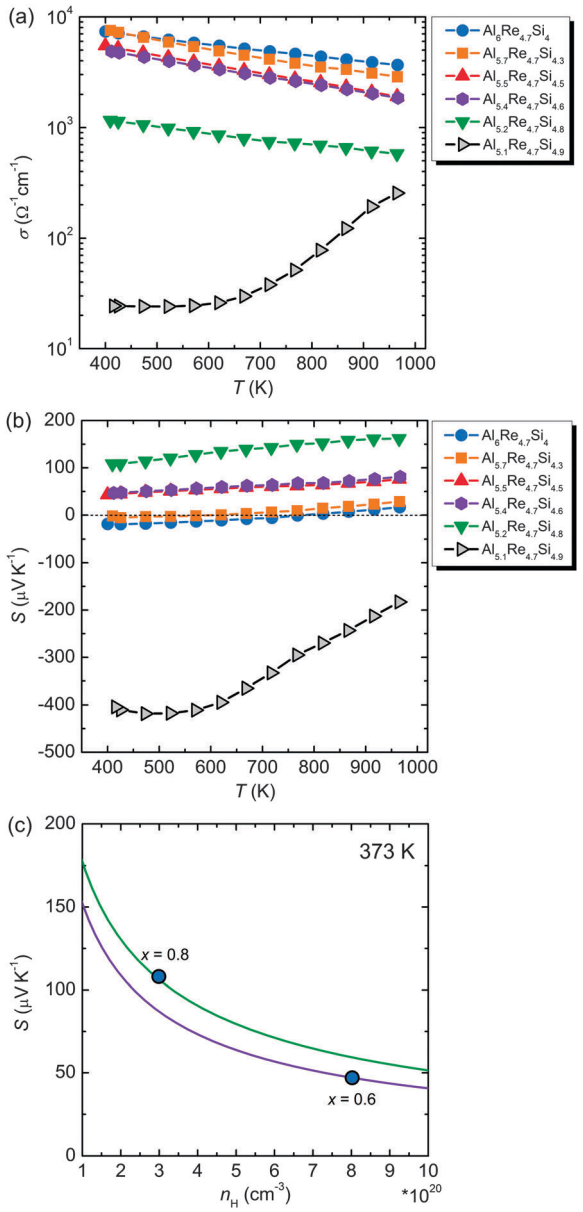

Fig. 7 (a) Electrical conductivity, σ, (b) Seebeck coefficient, S, for $Al_{6-x}Re_{4.7}Si_{4+x}$ (x = 0–0.9), and (c) Seebeck coefficient as a function of Hall carrier concentration, n_H, for $Al_{6-x}Re_{4.7}Si_{4+x}$ (x = 0.6 and 0.8). The solid lines show calculated S curves at 373 K, using a SPB model with $m^* = 1.6m_e$ (x = 0.6) and $2.1m_e$ (x = 0.8), respectively.

$$r_H = \frac{3}{2}F_{1/2}\frac{F_{-1/2}}{2F_0^2}, \quad (3)$$

$$F_j(\eta) = \int_0^\infty \frac{\varepsilon^j d\varepsilon}{1+\exp(\varepsilon-\eta)}, \quad (4)$$

where k_B, F_j, m^*, h, n, r_H, ε, and η are the Boltzmann constant, the Fermi integrals, the effective mass, the Planck constant, the chemical carrier concentration, the Hall factor, the reduced carrier energy, and the reduced chemical potential, respectively. The obtained m^* for $Al_{6-x}Re_{4.7}Si_{4+x}$ (x = 0.6 and 0.8) are $1.6m_e$ and $2.1m_e$, respectively, and these m^* are much heavier than that ($\sim 0.3m_e$) predicted by the calculation. Here, we note that the band degeneracy of N_v = 4 is expected in $Al_{6-x}Re_{4.7}Si_{4+x}$, therefore, the apparent heavy m^* will be reasonable and in such a case S can be enhanced with a higher carrier concentration of $\sim 10^{20}$ cm^{-3}.

On the other hand, the semiconducting sample with x = 0.9 shows a large negative S value of -400 μV K^{-1} at 400 K, indicating that E_F shifts to the conduction band edge because of an increase in the number of valence electrons. However, a dramatic decrease in $|S|$ above 600 K is observed as a result of the excitations of minority carriers, which is the same trend seen in σ.

The power factor, $S^2\sigma$, increases with increasing x up to x = 0.8, as shown in Fig. 8. By adjusting E_F close to the valence band edge, the highest $S^2\sigma$ of 1.65 mW m^{-1} K^{-2} with the highest S is obtained for the x = 0.8 sample as a p-type material. The n-type sample (x = 0.9) should be adjusted by further electron doping for higher $S^2\sigma$ because the carrier concentration is too low. This large power factor in the $Al_6Re_5Si_4$ phase is comparable to those of $TiSi_2$-type Al–Mn–Si[32] and $RuAl_2$.[12]

Fig. 9a–e show the total thermal conductivity, κ_{total}, the electron thermal conductivity, $\kappa_{electron}$, the phonon thermal conductivity, κ_{phonon}, the specific heat, C_P, and the thermal diffusivity, α, as a function of temperature. The $\kappa_{electron}$ was calculated using the Wiedemann–Franz law ($\kappa_{electron} = L\sigma T$). We estimated a Lorenz number using a model proposed by Kim *et al.*, L = 1.5 + exp[$-|S|/116$] × 10^{-8} V^2 K^{-2}.[39] The $\kappa_{electron}$ decreases with increasing x due to a decrease in σ. Because of the simple crystal structure, a relatively large κ_{phonon} is observed from 3.2 W m^{-1} K^{-1} to 9.2 W m^{-1} K^{-1} at 300 K. The κ_{phonon} decreases with increasing temperature because of Umklapp scattering. However, an unusual trend of increasing κ_{phonon} at high temperatures may be understood by the bipolar diffusion effect[40] brought about by excitations of both electrons and holes, judging from the results of the S. The κ_{phonon} seems to increase with increasing x. To obtain further insight, we measured the speed of sound, v_s, and calculated the Debye temperature, θ_D, for samples with x = 0–0.9, as listed in Table 1. Here, κ_{phonon} can be expressed as follows:

$$\kappa_{phonon} = \frac{1}{3}C_P{v_s}^2\tau_{phonon}, \quad (5)$$

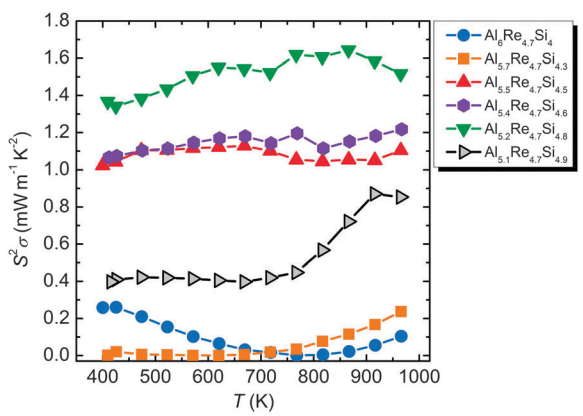

Fig. 8 Power factor, $S^2\sigma$, as a function of temperature for $Al_{6-x}Re_{4.7}Si_{4+x}$ (x = 0–0.9).

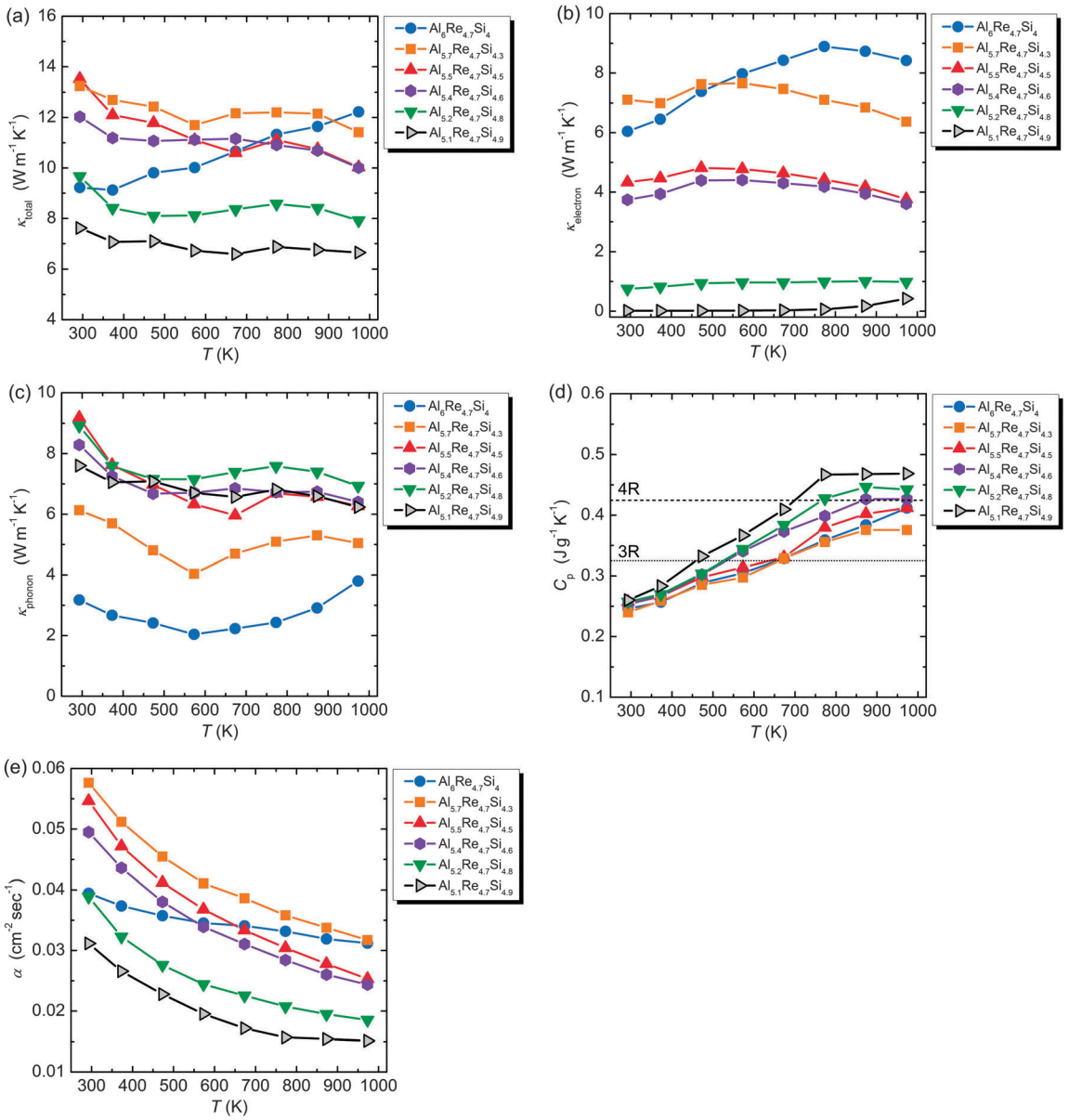

Fig. 9 (a) Total thermal conductivity, κ_{total}, (b) electron thermal conductivity, $\kappa_{electron}$, (c) phonon thermal conductivity, κ_{phonon}, (d) specific heat, C_P, and (e) thermal diffusivity, α, as a function of temperature for $Al_{6-x}Re_{4.7}Si_{4+x}$ (x = 0–0.9). The dotted and dashed lines represent the Dulong–Petit limit (3R) and 4R, respectively.

where τ_{phonon} is the phonon relaxation time. Apparently, there is no systematic trend in ν_s and θ_D to explain the composition dependence of κ_{phonon}. In this case, the degree of chemical disordering of Al/Si sites may influence τ_{phonon}; κ_{phonon} decreases with increasing contrast between Al and Si.

The dimensionless figure-of-merit, zT, is displayed in Fig. 10a. Except for x = 0, zT monotonically increases with increasing temperature. The maximum zT, zT_{max}, is observed at 973 K for all samples, and zT_{max} increases with increasing x up to x = 0.8. In the measured temperature range, the highest zT_{max} values of 0.19 as p-type and 0.12 as n-type at 973 K were determined for samples with x = 0.8 and 0.9, respectively. The present materials have a high melting point of approximately 2000 K, consequently zT will be enhanced at higher temperatures. To elucidate the optimal carrier concentration for zT, we calculated zT as a function of n_H within the SPB model,

Table 1 Speed of sound, ν_s, and Debye temperature, θ_D, for $Al_{6-x}Re_{4.7}Si_{4+x}$ (x = 0–0.9)

Sample	ν_s (m s^{-1})	θ_D (K)
x = 0	4.89 × 10^3	593
x = 0.3	5.03 × 10^3	611
x = 0.5	5.09 × 10^3	618
x = 0.6	5.09 × 10^3	619
x = 0.8	4.99 × 10^3	608
x = 0.9	4.68 × 10^3	570

as follows:

$$zT = \frac{S^2}{L + (\psi\beta)^{-1}}, \quad (6)$$

$$L = \frac{{k_B}^2}{e^2}\frac{3F_0F_2 - 4{F_1}^2}{{F_0}^2}, \quad (7)$$

$$\beta = \frac{\mu_0(m^*/m_e)^{3/2}T^{5/2}}{\kappa_{phonon}}, \quad (8)$$

$$\psi = \frac{8\pi e}{3}\left(\frac{2m_ek_B}{h^2}\right)^{3/2}F_0, \quad (9)$$

$$\mu_H = \mu_0\frac{F_{-1/2}}{2F_0}. \quad (10)$$

Here, we assume that μ_H decays T (degenerate behavior) at high temperatures and the constant n_H is used for a rough estimation of the zT curve at 973 K. Using the parameters m^* = 2.1(0.9)m_e, μ_H = 36(12) cm^2 V^{-1} s^{-1}, and κ_{phonon} = 8.9(7.0) W m^{-1} K^{-1} calculated using L = 1.88 × 10^{-8} (1.71 × 10^{-8}) V^2 K^{-2} at 373 K (at 973 K), the predicted zT curves at 373 K and 973 K are displayed in Fig. 10b. The zT curves are consistent with the experimental data, indicating that the obtained zT of 0.19 is close to the optimal zT value. To enhance the zT value for this compound, κ_{phonon} should be lowered by alloying and/or nanostructuring.

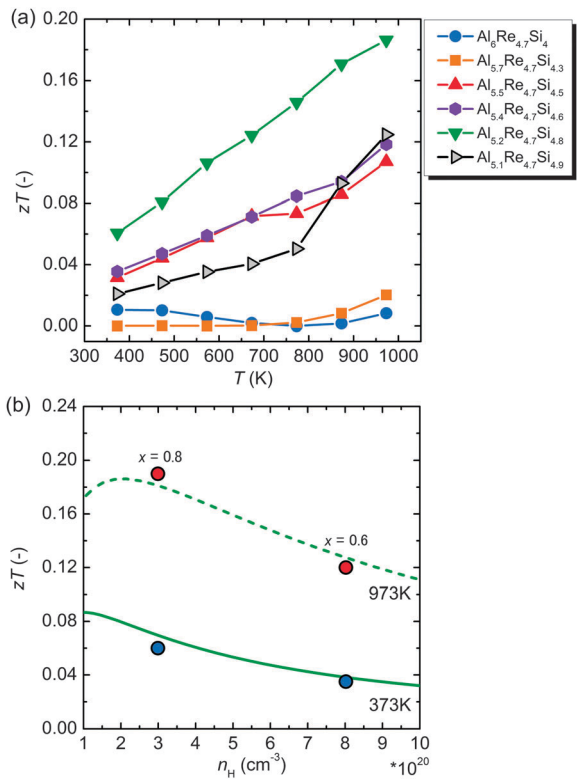

Fig. 10 (a) Dimensionless figure of merit, zT, as a function of temperature for $Al_{6-x}Re_{4.7}Si_{4+x}$ (x = 0–0.9), and (b) zT as a function of Hall carrier concentration for p-type $Al_{6-x}Re_{4.7}Si_{4+x}$ (x = 0.6 and 0.8). The solid and dashed lines show calculated zT curves at 373 K and 973 K, respectively.

5. Conclusions

The thermoelectric properties of $MoSi_2$-type intermetallic compounds $Al_{6-x}Re_{4.7}Si_{4+x}$ (x = 0–0.9) were systematically investigated in the temperature range from 373 K to 973 K. To clarify the electronic structure, a first-principles band structure calculation was performed for $ReAl_2$, ReAlSi, and $ReSi_2$. The calculation implied that this compound forms a narrow band gap of ~0.3 eV in the electronic density of states. Indeed, $Al_{6-x}Re_{4.7}Si_{4+x}$ (x = 0–0.8) samples behaved as degenerate semiconductors while $Al_{5.1}Re_{4.7}Si_{4.9}$ (x = 0.9) showed non-degenerate properties with a band gap of 0.53 eV. A large $S^2\sigma$ of 1.65 mW m^{-1} K^{-2} at 873 K was observed for the sample with x = 0.8 by adjusting the position of E_F. However, a relatively large κ_{phonon} was observed from 3.2 W m^{-1} K^{-1} to 9.2 W m^{-1} K^{-1} at 300 K because of the simple crystal structure. We confirmed that the increasing contrast between Al/Si can decrease the κ_{phonon}. The maximum zT reached 0.19 at 973 K for $Al_{5.2}Re_{4.7}Si_{4.8}$ (x = 0.8), whose value is close to that of the optimal zT determined using the SPB model.

Acknowledgements

This work was supported by KAKENHI Grant No. 24360262 and 26709051 from the Japan Society for the Promotion of Science.

References

1 G. J. Snyder and E. S. Toberer, *Nat. Mater.*, 2008, **7**, 105–114.
2 J. P. Heremans, V. Jovovic, E. S. Toberer, A. Saramat, K. Kurosaki, A. Charoenphakdee, S. Yamanaka and G. J. Snyder, *Science*, 2008, **321**, 554–557.
3 Y. Pei, X. Shi, A. D. LaLonde, H. Wang, L. Chen and G. J. Snyder, *Nature*, 2011, **473**, 66–69.
4 M. G. Kanatzidis, *Chem. Mater.*, 2010, **22**, 648–659.
5 Y. Pei, A. D. LaLonde, S. Iwanaga and G. J. Snyder, *Energy Environ. Sci.*, 2011, **4**, 2085–2090.
6 M. Christensen, S. Johnsen and B. B. Iversen, *Dalton Trans.*, 2010, **39**, 978–992.
7 G. S. Nolas, D. T. Morelli and T. M. Tritt, *Annu. Rev. Mater. Sci.*, 1999, **29**, 89–116.
8 E. S. Toberer, A. Zevalkink and G. J. Snyder, *J. Mater. Chem.*, 2011, **21**, 15843–15852.
9 Y. Takagiwa and K. Kimura, *Sci. Technol. Adv. Mater.*, 2014, **15**, 044802.
10 D. Mandrus, V. Keppens, B. C. Sales and J. L. Sarrao, *Phys. Rev. B: Condens. Matter Mater. Phys.*, 1998, **58**, 3712–3716.
11 S. Takahashi, H. Muta, K. Kurosaki and S. Yamanaka, *J. Alloys Compd.*, 2010, **493**, 17–21.
12 Y. Takagiwa, Y. Matsubayashi, A. Suzumura, J. T. Okada and K. Kimura, *Mater. Trans., JIM*, 2010, **51**, 988–993.

13 Y. Amagai, A. Yamamoto, C.-H. Lee, H. Ohara, K. Ueno, T. Iida and Y. Takanashi, *Papers of Technical Meeting on Frontier Technology and Engineering*, IEE Japan, 2005, vol. FTE-05, p. 41, in Japanese.
14 Y. Takagiwa, J. T. Okada and K. Kimura, *J. Alloys Compd.*, 2010, **507**, 364–369.
15 V. Ponnambalam, G. Lehr and D. T. Morelli, *J. Mater. Res.*, 2011, **26**, 1907–1912.
16 Y. Takagiwa, J. T. Okada and K. Kimura, *J. Electron. Mater.*, 2011, **40**, 1067–1072.
17 Y. Takagiwa, K. Kitahara and K. Kimura, *J. Appl. Phys.*, 2013, **113**, 023713.
18 Y. Takagiwa, K. Kitahara and K. Kimura, *Mater. Trans., JIM*, 2013, **54**, 953–957.
19 N. Sato, Y. Matsuura, K. Kitahara, Y. Takagiwa and K. Kimura, *J. Alloys Compd.*, 2014, **585**, 455–459.
20 Y. Amagai, A. Yamamoto, T. Iida and Y. Takanashi, *J. Appl. Phys.*, 2004, **96**, 5644–5648.
21 Y. Takagiwa, K. Kitahara, Y. Matsubayashi and K. Kimura, *J. Appl. Phys.*, 2012, **111**, 123707.
22 M. Wagner, R. Cardoso-Gil, N. Oeschler, H. Rosner and Y. Grin, *J. Mater. Res.*, 2011, **26**, 1886–1893.
23 D. Kasinathan, M. Wagner, K. Koepernik, R. Cardoso-Gil, Y. Grin and H. Rosner, *Phys. Rev. B: Condens. Matter Mater. Phys.*, 2012, **85**, 035207.
24 N. Haldolaarachchige, W. A. Phelan, Y. M. Xiong, R. Jin, J. Y. Chan, S. Stadler and D. P. Young, *J. Appl. Phys.*, 2013, **113**, 083709.
25 M. Wagner-Reetz, R. Cardoso-Gil, M. Schmidt and Y. Grin, *J. Solid State Chem.*, 2014, **215**, 260–264.
26 N. Haldolaarachchige, A. B. Karki, W. Adam Phelan, Y. M. Xiong, R. Jin, J. Y. Chan, S. Stadler and D. P. Young, *J. Appl. Phys.*, 2011, **109**, 103712.
27 B. Ramachandran, K. Z. Syu, Y. K. Kuoa, A. A. Gippius, A. V. Shevelkov, V. Yu. Verchenko and C. S. Lue, *J. Alloys Compd.*, 2014, **608**, 229–234.
28 Y. Takagiwa, Y. Matsuura and K. Kimura, *J. Electron. Mater.*, 2014, **43**, 2206–2211.
29 M. Wagner-Reetz, R. Cardoso-Gil and Y. Grin, *J. Electron. Mater.*, 2014, **43**, 1857–1864.
30 D. C. Fredrickson, S. Lee and R. Hoffmann, *Inorg. Chem.*, 2004, **43**, 6159–6167.
31 T. Takeuchi, Y. Toyama, A. Yamamoto, H. Hazama and R. Asahi, *Mater. Trans., JIM*, 2010, **51**, 1127–1135.
32 A. Yamamoto, H. Miyazaki and T. Takeuchi, *J. Appl. Phys.*, 2014, **115**, 023708.
33 A. Yamamoto, H. Miyazaki, M. Inukai, Y. Nishino and T. Takeuchi, *Jpn. J. Appl. Phys.*, 2015, **54**, 071801.
34 Y. B. Kuz'ma and V. V. Milyan, *Neorg. Mater.*, 1977, **13**, 926–927.
35 R. Tamura, T. Asao and S. Takeuchi, *Phys. Rev. Lett.*, 2001, **86**, 3104–3107.
36 http://www.advancesoft.jp/product/advance_phase/.
37 T. Siegrist, F. Hulliger and G. Travaglini, *J. Less-Common Met.*, 1983, **92**, 119–129.
38 A. Zevalkink, E. S. Toberer, W. G. Zeier, E. Flage-Larsen and G. J. Snyder, *Energy Environ. Sci.*, 2011, **4**, 510–518.
39 H.-S. Kim, Z. M. Gibbs, Y. Tang, H. Wang and G. J. Snyder, *APL Mater.*, 2015, **3**, 041506.
40 H. J. Goldsmid, *The Thermal Properties of Solids*, Dover Publications, New York, 1965.